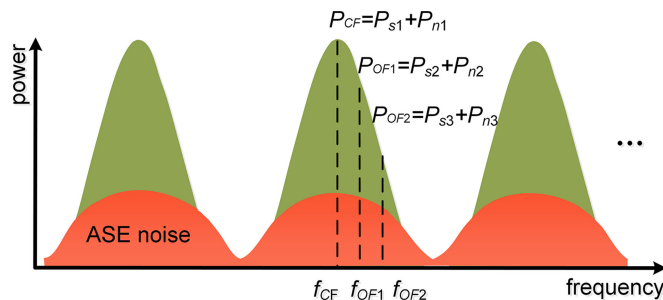# Reference Optical Spectrum Based In-Band OSNR Monitoring Method for EDFA Amplified Multispan Optical Fiber Transmission System With Cascaded Filtering Effect

Guo Yin
Sheng Cui
Changjian Ke
Deming Liu

Reference Optical Spectrum Based In-Band OSNR Monitoring Method for EDFA Amplified Multispan Optical Fiber Transmission System With Cascaded Filtering Effect

Guo Yin [1,2] **Sheng Cui** [1,2] **Changjian Ke** [1,2] **and Deming Liu**[1,2]

[1]School of Optical and Electrical Information, Huazhong University of Science and Technology, Wuhan 430074, China
[2]National Engineering Laboratory for Next Generation Internet Access System, Wuhan 430074, China

Abstract: The reference optical spectrum (ROS) based in-band optical signal-to-noise-ratio (OSNR) monitoring methods are accurate and inherently robust to fiber chromatic dispersion and polarization mode dispersion. They are also very simple and suitable to be deployed ubiquitously in the transmission system. In this paper, a ROS-based in-band OSNR monitoring method is proposed for erbium doped fiber amplifier (EDFA) amplified multispan dense wavelength division multiplexing systems with cascaded filtering effect (CFE) caused by cascaded add-drop filters or wavelength selective switches. In such systems, the optical signal as well as the optical noise may experience significant CFE making the ROS-based methods proposed before ineffective. The new method solves this problem and performs very well for OSNR in the range of 10–30 dB when the fiber nonlinear effect and nonideal filtering effect are present. The OSNR monitor based on the new method is also more convenient to use as only one-time calibration is required when used at different monitoring locations along the optical link.

Index Terms: Optical signal to noise ratio (OSNR), optical performance monitoring (OPM), optical spectrum (OS), cascaded filtering effect (CFE).

1. Introduction

Optical networks rely on optical performance monitoring (OPM) techniques to ensure robust transmission [1]. Among the list of OPM parameters, optical signal-to-noise ratio (OSNR) is one of the key and indispensable aspects [1]–[6]. Traditional standardized OSNR monitoring method is based on the linear interpolation of the noise level from the spectral gaps between signals. However, this method is not adequate for the dense wavelength division multiplexing (DWDM) transmission systems with cascaded filtering effect (CFE) caused by intermediate nodes consisting of optical filtering elements, because the out-of-band noise may be highly suppressed. To solve this problem,
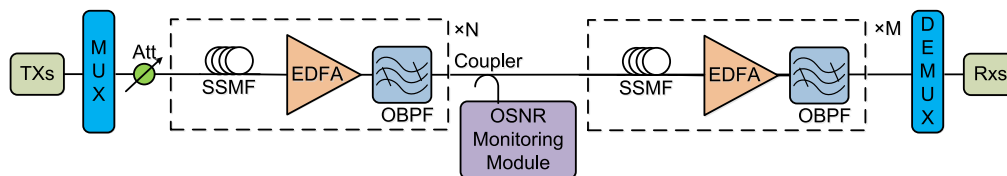
Fig. 1. The Schematic diagram of the setup of the EDFA amplified multi-span DWDM system. Tx: transmitter, Rx: receiver, SSMF: standard single mode fiber, EDFA: erbium doped fiber amplifier, OBPF: multichannel optical band pass filter. The OSNR monitoring module can be placed after any intermediate node.

many in-band OSNR monitoring methods have been proposed [2]–[6]. These methods can be classified into two main types. The first type utilizes linear or nonlinear optical schemes, such as polarization-nulling techniques [2], an optical delay interferometer (ODI) [3], a non-linear loop mirror [4], a fiber parametric device [5], [6] or an optical detector designed for two-photo absorption [7]. While the second type utilizes advanced digital signal processing (DSP) embedded in the coherent optical receivers [8]–[10]. Each of these methods has some merits but also some drawbacks. For the first type of methods, they have no bit rate limits and are relatively simple, thus cost-effective for wide deployment. But some of them are not effective to polarization-multiplexed (PM) signals, while the others may be sensitive to chromatic dispersion (CD), polarization mode dispersion (PMD), CFE and nonlinear effect (NLE). For the second type of methods, they can be robust to CD, PMD and NLE thanks to the advanced DSP algorithms, but they can measure OSNR only at the location of the coherent receiver. To deploy such OSNR monitors widely across the network including the intermediate nodes will be too costly and impractical.

Recently reference optical spectrum (ROS) based in-band OSNR monitoring methods have been intensively studied [11]–[16]. These methods utilize widely-deployed conventional optical spectrum analyzers (OSA) [11] or just simple optical band-pass filters (OBPFs) in combination with optical power meters [14]. They rely on a detailed spectral comparison of the ROS without noise which is measured at or near the transmitter with the one measured at the desired OSNR monitoring point. When it is inconvenient to undertake a ROS measurement at or near the transmitter, the ROS can also be directly retrieved from the ones measured at the monitoring point using machine-learning techniques [17]. The ROS based methods are not only effective to PM and superchannel signals, but also robust to CD, PMD and NLE. But most of these methods are still sensitive to the CFE [15]. In [15] an improved ROS based method which is insensitive to CFE is proposed. But the method doesn't consider the CFE on the in-band noise spectrum shape, thus the performance degrades for erbium doped fiber amplifier (EDFA) amplified multi-span systems where the optical noise as well as signal may pass through a number of filtering elements and experience significant CFE. In this paper we proposed a method to solve this problem. Extensive numerical simulations show that our method performs very well even when the aforementioned CFE insensitive method fails.

2. Principle of Operation

The working principle of our method is schematically shown in Figs. 1 and 2. Fig. 1 shows the typical setup of the EDFA amplified multi-span DWDM system. The multi-channel OBPFs are used to represent the intermediate filtering elements in the optical nodes. The OSNR monitoring module can be placed after any intermediate node utilizing a small portion of the optical signal tapped off the main link with an optical coupler. Here OSNR monitoring module is placed after N span. Fig. 2(a) shows the ROS without noise measured at the transmitter. The ROS shape and the power ratios $R_1 = P_2/P_1$ and $R_2 = P_3/P_1$ are determined by the type of optical signal. Here $P_{1,2,3}$ are the signal spectral powers measured at the frequencies of f_{CF}, f_{OF1} and f_{OF2}. Here f_{CF} represents the ROS center frequency and $f_{OF1,2}$ represent two offset frequencies from f_{CF}. For comparison, Fig. 2(b) and (c) shows the signal optical spectrum (OS) with accumulated ASE noise for the systems when CFE is not present and present, respectively. For the former case the incoherent noise has a nearly flat spectrum within the interesting bandwidth, so the in-band noise power P_n can be estimated by
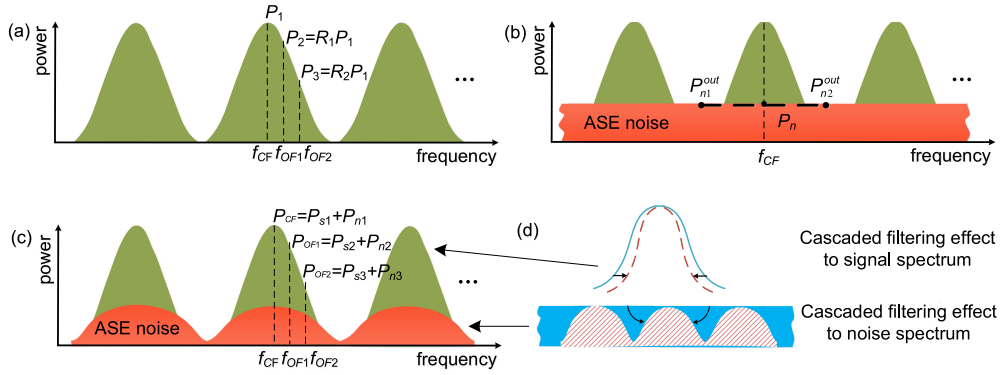
Fig. 2. The Schematic diagram of the working principles of the in-band OSNR monitoring methods. The ROS without noise measured at the transmitter (a). The signal optical spectrum with accumulated ASE noise when CFE is not present (b) and present (c). The influence of CFE on the signal and noise spectra (d).

the linear interpolation between the out-of-band noise powers P_{n1}^{out} and P_{n2}^{out}. This method becomes ineffective when CFE is present because the out-of-band noise may be greatly suppressed by CFE as shown in Fig. 2(c). To solve the above problem, the spectral powers at f_{CF}, f_{OF1} and f_{OF2} are measured. As shown in Fig. 2(c) the measured spectral powers can be expressed as:

$$P_{CF} = P_{s1} + P_{n1},$$

$$P_{OF1} = P_{s2} + P_{n2} = R_1 \alpha^N P_{s1} + P_{n2},$$

$$P_{OF2} = P_{s3} + P_{n3} = R_2 \beta^N P_{s1} + P_{n3}. \tag{1}$$

where $P_{s1,s2,s3}$ represent the signal powers (not including the noise), while $P_{n1,n2,n3}$ represent the noise powers. The weighting factor α^N and β^N are introduced to depict the CFE on the signal OS. Here α and β are the spectral transmission coefficients of the intermediate filtering elements at f_{OF1} and f_{OF2}, respectively. In [15], the in-band noise spectrum is assumed to be flat. In other words $P_{n1,n2,n3}$ are assumed to be equal to each other. In this case (1) can be simplified into the following equations proposed in [15]:

$$P_{CF} = P_{s1} + P_n,$$

$$P_{OF1} = P_{s2} + P_{n2} = R_1 \alpha^N P_{s1} + P_n,$$

$$P_{OF2} = P_{s3} + P_{n3} = R_2 \beta^N P_{s1} + P_n. \tag{2}$$

By solving (2), we can obtain N, P_{s1} and P_n and thus calculate the in in-band OSNR by:

$$OSNR = \gamma \frac{P_{s1}}{P_n} \tag{3}$$

where the calibration parameter γ is determined by the OBPF bandwidth and signal bandwidth and should be calibrated to balance the positive and negative OSNR estimation errors.

In fact the in-band noise spectrum has a graded profile as shown in Fig. 2(c) because real optical filters have a graded profile, such as a super-Gaussian profile, instead of a rectangular one. In other words $P_{n1} \neq P_{n2} \neq P_{n3}$ especially when the two offset frequencies are close to the OS edge. Fig. 2(d) schematically shows the influence of CFE on the signal and noise spectra, respectively. The signal OS becomes narrower, while the noise spectrum becomes non-flat like the spectral shape of the filter.

Assuming the EDFAs totally compensate the span loss and have the same noise figure, at the monitoring point the accumulated noise spectral power at f_{CF} is given by $P_{n1} = N P_{ASE}$. Here we stress that P_{ASE} is defined as the noise power contributed by each EDFA at f_{CF}. While for the noise
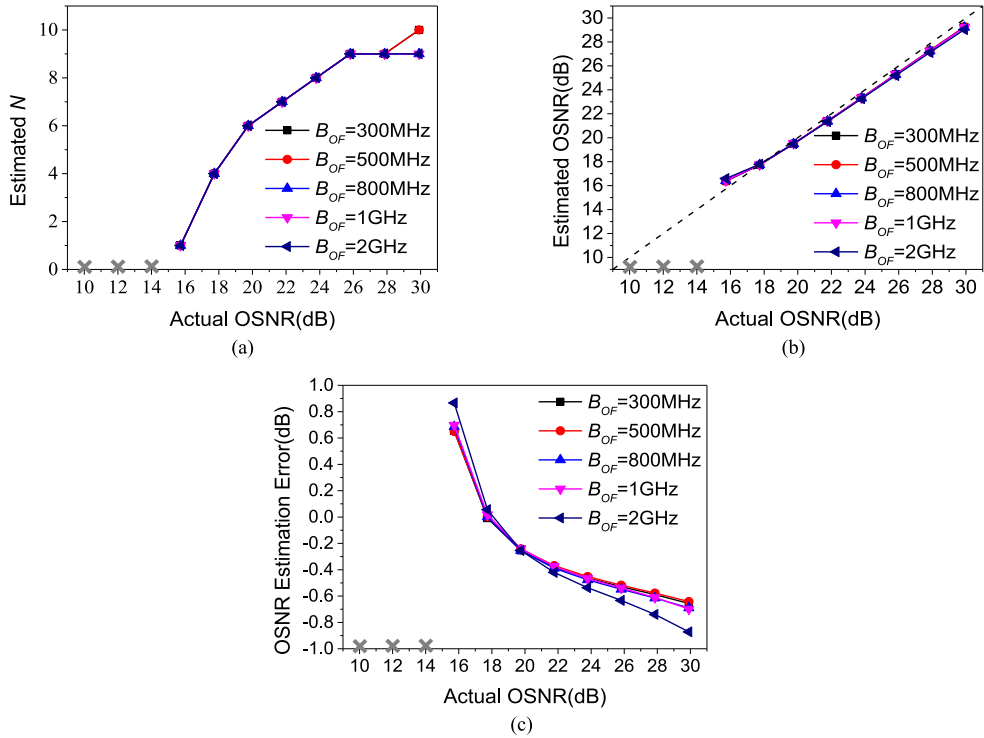
Fig. 3. The OSNR monitoring results obtained with method 1. The curves of the estimated N (a), estimated OSNR (b) and OSNR estimation error (c) against the actual OSNR.

powers at the two offset frequencies, they are attenuated by CFE. It is obvious that the further away the noise is generated from the monitoring point, the larger CFE it experience as the noise has to pass through more filtering elements before reaching the monitoring point. So considering CFE on the in-band noise spectrum profile, the noise spectral powers $P_{n2,n3}$ at f_{OF1} and f_{OF2} can be rewritten as:

$$P_{n2} = \alpha P_{ASE} + \alpha^2 P_{ASE} + \cdots + \alpha^N P_{ASE} = \frac{\alpha - \alpha^{N+1}}{(1-\alpha)} P_{ASE} = \frac{\alpha - \alpha^{N+1}}{(1-\alpha)N} P_{n1},$$

$$P_{n3} = \beta P_{ASE} + \beta^2 P_{ASE} + \cdots + \beta^N P_{ASE} = \frac{\beta - \beta^{N+1}}{(1-\beta)} P_{ASE} = \frac{\beta - \beta^{N+1}}{(1-\beta)N} P_{n1}. \quad (4)$$

Substituting (4) into (1), the following equations can obtained:

$$P_{CF} = P_{s1} + P_{n1},$$

$$P_{OF1} = R_1 \alpha^N P_{s1} + \frac{\alpha - \alpha^{N+1}}{(1-\alpha)N} P_{n1},$$

$$P_{OF2} = R_2 \beta^N P_{s1} + \frac{\beta - \beta^{N+1}}{(1-\beta)N} P_{n1}. \quad (5)$$

By solving (5), we can obtain N, P_{s1} and P_{n1} and then calculate the in-band OSNR using (3) after replacing P_n with P_{n1}.

3. Numerical Simulations and Results

First we investigate the performance of the two methods proposed by [15] and this paper in the EDFA amplified multi-span system shown in Fig. 1. The two methods are referred as method
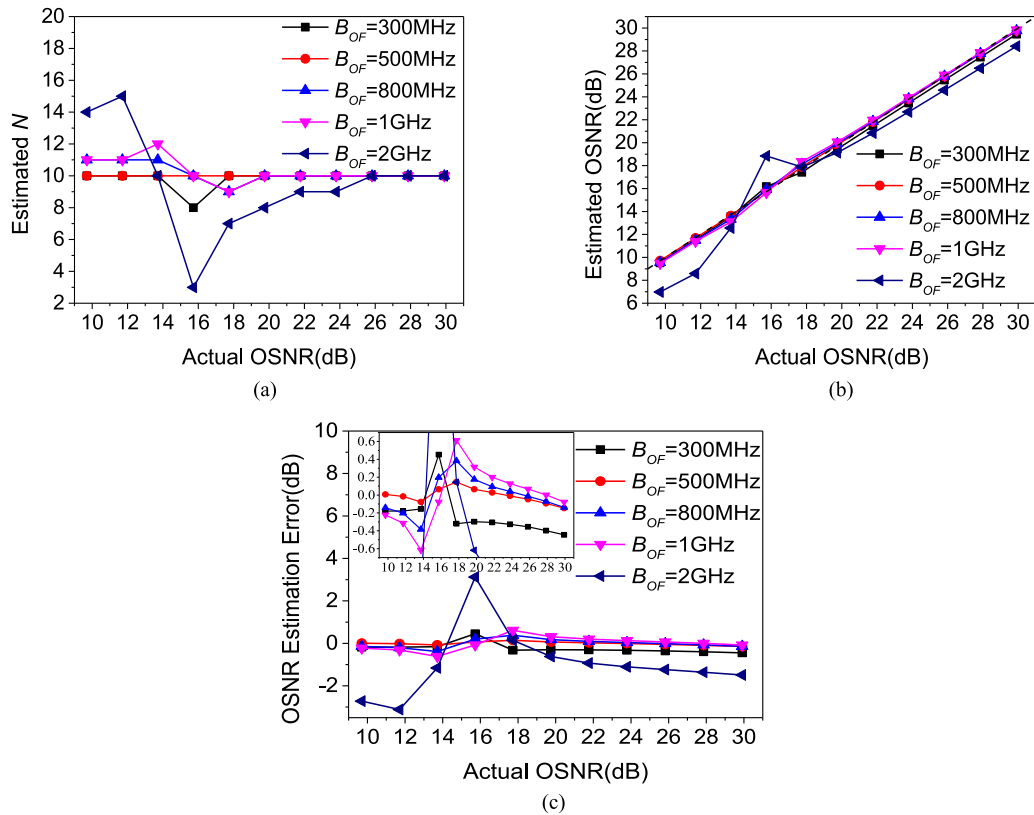
Fig. 4. The OSNR monitoring results obtained with method 2 when $N = 10$. The curves of the estimated N (a), estimated OSNR (b) and OSNR estimation error (c) against the actual OSNR.

1 and method 2, respectively. The numerical simulations are based on VPI TransmissionMaker 9.1. The signal under test is 25 GBaud dual-polarization QPSK signal. The span length is set to 80 km. The EDFA fully compensate the span loss and has a noise figure of 4. In such system the noise also experience CFE as the noise along with the signal is filtered by multiple OBPFs before reaching the monitoring point. A realistic 50 GHz 3 dB bandwidth super-Gaussian OBPF model has been implemented. The two spectral power measurement offset frequencies are set at $f_{OF1} = f_{CF} + 20\,\text{GHz}$ and $f_{OF2} = f_{CF} + 23.5\,\text{GHz}$ which are optimized results according to [15]. The spectral powers P_{CF}, P_{OF1} and P_{OF2} are measured using the method proposed in [15] which utilizes low-cost coherent receptions and finer electrical filters to replace the required sub-GHz bandwidth optical filters which are expensive and not commercially available at present. The OSNR is varied from 10 dB to 30 dB by changing the launched signal power.

Fig. 3 shows the results obtained with method 1 when $N = 10$. The bandwidth of the electrical filters used in RF power measurement (B_{OF}) is varied in the range of 300 MHz to 2 GHz. Fig. 3(a) shows that the estimated N against the actual one for different OSNRs. As we can see the estimated N deviates grossly from the real value and is close to 10 only when OSNR is very high. When OSNR $< 16\,\text{dB}$, N has no positive solutions according to (2). The reason is that the assumption made by method 1 is no longer valid in these cases. We note that in Fig. 3(a) and following figures the cases when (2) have no valid solutions are represented by crosses. Fig. 3(b) shows the estimated OSNR against the actual OSNR. Ideally the curves should be a set of 45 degrees straight lines as the estimated OSNR should be equal to the actual OSNR. As we can see the curves obtained have good linearity and are close to the ideal one represented by the dashed line for OSNR above 16 dB. Fig. 3(c) shows that the maximal OSNR estimation error is below 0.65 dB when $B_{OF} = 500\,\text{MHz}$
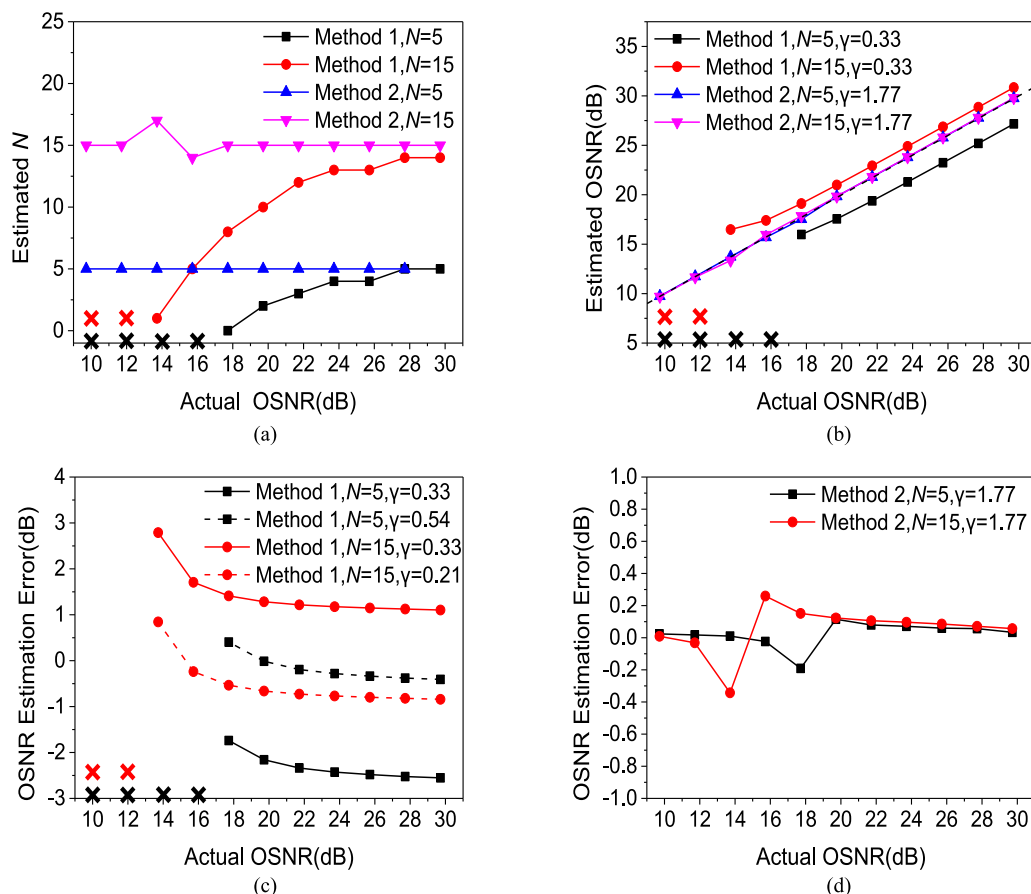
Fig. 5. The OSNR monitoring results obtained with the two methods when $N = 5$ and 15. The curves of the estimated N (a), estimated OSNR (b), method 1 OSNR estimation error (c) and method 2 OSNR estimation error (d) against the actual OSNR.

for OSNR $\geq$ 16 dB. But because N has no solutions when OSNR $<$ 16 dB neither can OSNR be calculated in these cases. Finally it is noteworthy γ is set at 0.33 so that the magnitudes of the errors on the positive and negative sides are equal to each other as shown in Fig. 3(c).

Fig. 4 shows the results obtained with method 2. It is obvious that method 2 works even when method 1 fails. Fig. 4(a) shows that the estimated N has correct solutions for OSNR in the range of 10-30 dB when $B_{OF} = 500$ MHz. Fig. 4(b) and (c) show the estimated OSNR and estimation error against the actual OSNR. After calibration and setting $\gamma = 1.77$ the maximal OSNR estimation error is below 0.15 dB, which is 0.5 dB smaller than that obtained with method 1. It is noteworthy that γ used in Fig. 4 is different from that in Fig. 3 because the two methods have different estimation errors. So the optimal γ balancing the positive and negative errors is also different.

To further investigate the performance of the two methods for systems with different spans, they are applied in systems with $N = 5$ and 15, respectively. B_{OF} is set at 500 MHz in the following simulation. For the convenience of comparison the results obtained with method 1 and 2 are simultaneously shown in Fig. 5. As we can see from Fig. 5(a) with method 1 the estimated N deviates grossly from the real N at low OSNR while with method 2 the estimated N is very accurate for all the cases. Fig. 5(b) shows that with method 1 there exists a gap between the curves corresponding to the estimated and actual OSNR values. Here γ is still equal to 0.33 obtained when $N = 10$. It means γ should be re-calibrated when the OSNR monitoring module is deployed at different locations. As shown in Fig. 5(c) after re-calibration and setting $\gamma = 0.54$ and $\gamma = 0.21$
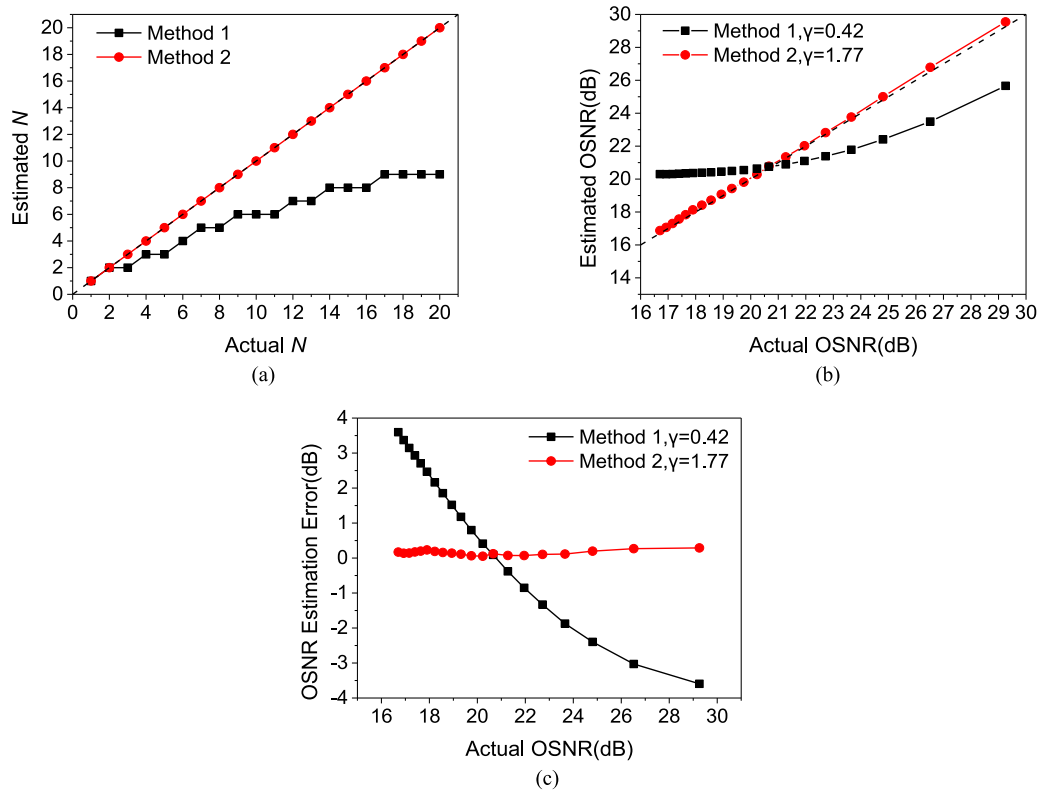
Fig. 6. The OSNR monitoring results obtained with the two methods when *N* is varied from 1 to 20. The curves of the estimated *N* (a), estimated OSNR (b) and OSNR estimation error (c) against the actual OSNR.

for $N = 5$ and 15, respectively, to balance the magnitude of the positive and negative errors, the maximal OSNR estimation error can be reduced from 3 to 1 dB. On the contrary, with method 2 the OSNR estimation error is still very small and below 0.3 dB with the same $\gamma (= 1.77)$ for $N = 10$. So no recalibration is needed when using method 2 at different monitoring points.

To investigate the re-calibration problem further, the OSNR monitoring module is placed at different optical nodes along the optical link. Fig. 6 shows the results obtained with method 1 and 2 when the span number before the monitoring point is varied from 1 to 20 with step of 1 while the other parameters keep the same. In this case OSNR will degenerate with increasing *N* as the result of accumulated ASE noise. Fig. 6(a) shows that using method 1 the estimated *N* is correct only when *N* is smaller than 3. While with method 2, the estimated *N* keeps correct for all monitoring locations. Fig. 6(b) shows that even after re-calibration and setting $\gamma = 0.42$ to balance the positive and negative errors the OSNR estimated with method 1 still deviates grossly from the actual values and the maximal OSNR estimation error is larger than 3.5 dB as shown in Fig. 6(c). While method 2 performs well for *N* in the range of 1 to 20 even using the same $\gamma (= 1.77)$ for $N = 10$. As Fig. 6(c) shows the OSNR estimation error is below 0.3 dB with the same γ. This means that method 2 is more accurate and convenient to use at monitoring points as it only requires one-time calibration.

To further investigate the impact of NLE on the performance of method 2 we varied the launched signal power. Fig. 7 shows the estimated results when the launch power is 0 dBm and 4 dBm, respectively. For comparison, the results obtained when NLE is not present are also shown in the figure. As we can see the estimated *N* keeps correct in all cases. Fig. 7(b) shows that when NLE is present the maximal OSNR estimation error is increased from 0.25 to 0.5 dB for the launched
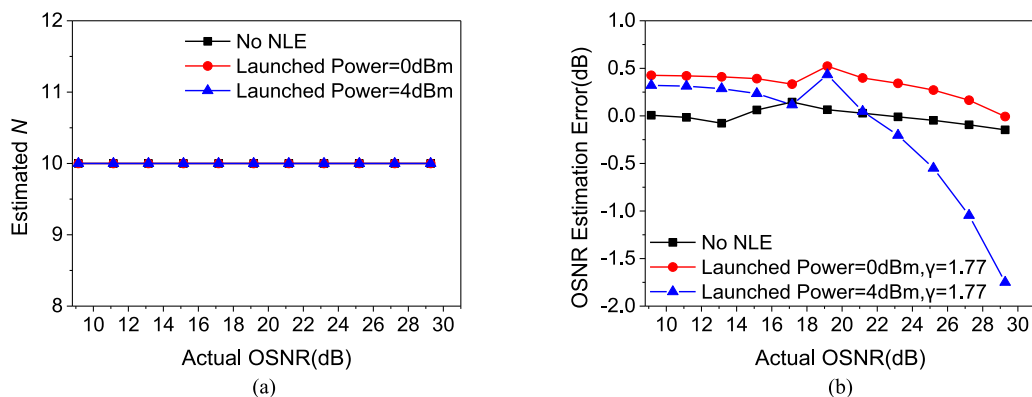
Fig. 7. The OSNR monitoring results obtained with method 2 when N is 10 and fiber nonlinear effect is present. The curves of the estimated N (a) and OSNR estimation error (b) against the actual OSNR.

TABLE 1

Combinations of f_{OF1} and f_{OF2} Used in Spectral Power Measurement

	f_{OF1}	f_{OF2}	γ
Scheme 1	f_{CF} +20GHz	f_{CF} +23.5GHz	1.77
Scheme 2	f_{CF} +19GHz	f_{CF} +22.5GHz	1.69
Scheme 3	f_{CF} +18GHz	f_{CF} +21.5GHz	1.65

power of 0 dBm. When the launched power is increased to 4 dBm the maximal estimation error increases to 1.8 dB at OSNR $=$ 30 dB because in this extreme high OSNR case the noise power is very low so the NLE induced spectrum broadening which affects $P_{n2,n3}$ becomes unneglectable. But even in this case the estimation error is still lower than 0.5 dB when OSNR is in the interesting range of 10 to 25 dB.

The influence of non-ideal filtering effect due to manufacture tolerance, temperature drift or aging problems on the performance of method 2 is also investigated. The results obtained with different combinations of f_{OF1} and f_{OF2} as listed in Table 1 are shown Fig. 8. In Fig. 8(a) the center frequency (CF) of the 10 OBPFs is shifted by $\pm$3 GHz. The performance of the three spectral power measurement schemes is compared (γ is calibrated individually assuming the non-ideal filtering effect is not present). As we can see with scheme 1 (the original one) the OSNR estimation error increases to 4.5 dB when OSNR is close to 10 dB. In scheme 2 f_{OF1} and f_{OF2} are moved toward f_{CF} to mitigate the non-ideal filtering effect, the maximal error can be reduced to 1 dB. In scheme 3 f_{OF1} and f_{OF2} are moved closer to f_{CF}, but the maximal error increases to 2 dB because R_1 and R_2 become too large which reduces the monitor's sensitivity to noise [14]. So the best performance can be achieved with scheme 2. In Fig. 8(b) the bandwidth (BW) of the 10 OBPFs is varied by $\pm$3 GHz. As we can see, with scheme 2, the maximal error is also lower than 1 dB. In Fig. 8(c) both the CF and BW of the filters are changed. The odd number OBPFs have CF-3 GHz and BW $+$ 3 GHz, while the even number OBPFs have CF $+$ 3 GHz and BW-3 GHz. Scheme 2 still achieved the best performance and with it the maximal error is lower than 1.5 dB when OSNR is in the interesting range of 10 to 25 dB. It is obvious that compared to NLE, non-ideal filtering effect is the primary reason for the degradation of the estimation accuracy.
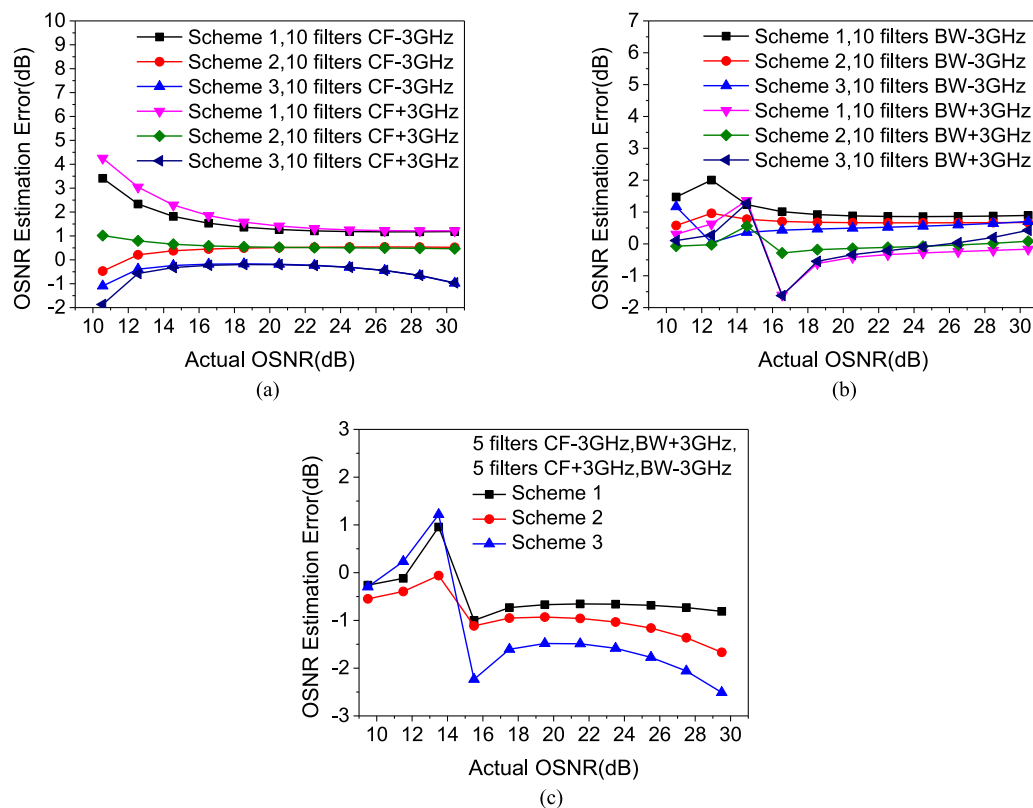
Fig. 8. The OSNR monitoring results obtained with method 2 when $N = 10$ and non-ideal filtering effect is present. The OSNR estimation error against the actual OSNR when the center frequency of the OBPFs are varied by ± 3 GHz (a), the bandwidth of the OBPFs are varied by ± 3 GHz (b) and the center frequency and bandwidth of the OBPFs are varied simultaneously (c).

4. Conclusion and Discussions

We have demonstrated that in the EDFA amplified multi-span DWDM systems CFE on the noise may greatly affect the performance of the ROS based methods and even may make them invalid when OSNR is lower than 16 dB. But with the method proposed the OSNR and the magnitude of CFE represented by N can still be very accurately estimated. This method is also easier to use at different monitoring points as only one-time calibration is required. The impact of NLE and non-ideal filtering elements are also investigated and it is demonstrated that this method is robust to NLE and non-ideal filtering effect. Comparatively non-ideal filtering effect is the primary reason that affects the estimation accuracy.

References

[1] Z. Dong, F. N. Khan, Q. Sui, K. Zhong, C. Lu, and A. P. T. Lau, "Optical performance monitoring: A review of current and future technologies," *J. Lightw. Technol.*, vol. 34, no. 2, pp. 525–543, Jan. 2016.
[2] J. H. Lee, D. K. Jung, C. H. Kim, and Y. C. Chung, "OSNR monitoring technique using polarization-nulling method," *IEEE Photon. Technol. Lett.*, vol. 13, no. 1, pp. 88–90, Jan. 2001.
[3] X. Liu, Y. H. Kao, S. Chandrasekhar, I. Kang, S. Cabot, and L. L. Buhl, "OSNR monitoring method for OOK and DPSK based on optical delay interferometer," *IEEE Photon. Technol. Lett.*, vol. 19, no. 15, pp. 1172–1174, Aug. 2007.
[4] R. Adams, M. Rochette, T. T. Ng, and B. J. Eggleton, "All-optical in-band OSNR monitoring at 40 Gb/s using a nonlinear optical loop mirror," *IEEE Photon. Technol. Lett.*, vol. 18, no. 3, pp. 469–471, Feb. 2006.
[5] T. T. Ng, J. L. Blows, M. Rochette, J. A. Bolger, I. Littler, and B. J. Eggleton, "In-band OSNR and chromatic dispersion monitoring using a fibre optical parametric amplifier," *Opt. Exp.*, vol. 13, no. 14, pp. 5542–5552, Jul. 2005.

[6] C. Sheng, S. Sun, L. Li, J. Li, Q. You, and D. Liu, "All-optical in-band optical signal-to-noise monitoring method based on degenerated four-wave mixing," *IET Optoelectron.*, vol. 6, no. 2, pp. 107–109, Apr. 2012.

[7] S. Wielandy, M. Fishteyn, and B. Zhu, "Optical performance monitoring using nonlinear detection," *J. Lightw. Technol.*, vol. 22, no. 3, pp. 784–793, Mar. 2004.

[8] M. S. Faruk, Y. Mori, and K. Kikuchi, "In-band estimation of optical signal-to-noise ratio from equalized signals in digital coherent receivers," *IEEE Photon. J.*, vol. 4, no. 1, pp. 1–9, Feb. 2014.

[9] D. Zhao, L. Xi, X. Tang, W. Zhang, Y. Qiao, and X. Zhang, "Periodic training sequence aided in-band OSNR monitoring in digital coherent receiver," *IEEE Photon. J.*, vol. 6, no. 4, pp. 1–8, Aug. 2014.

[10] L. Dou *et al.*, "An accurate nonlinear noise insensitive OSNR monitor," in *Proc. Opt. Fiber Commun. Conf. (Opt. Soc. Amer., 2016)*, Mar. 2016, Paper W3A. 5.

[11] D. Gariépy, G. He, and G. W. Schinn, "Non-intrusive measurement of in-band OSNR of high bitrate polarization-multiplexed signals," *Opt. Fiber Technol.*, vol. 17, no. 5, pp. 518–522, Oct. 2011.

[12] D. Gariépy, S. Searcy, G. He, and S. Tibuleac, "Non-intrusive OSNR measurement of polarization-multiplexed signals with spectral shaping and subject to fiber non-linearity with minimum channel spacing of 37.5 GHz," *Opt. Exp.*, vol. 24, no. 18, pp. 20156–20166, Sep. 2016.

[13] D. Gariépy, S. Searcy, G. He, and S. Tibuleac, "Demonstration of non-intrusive in-band OSNR measurement technique for PM-16 QAM signals with spectral shaping and subject to fiber nonlinearity," in *Proc. Opt. Fiber Commun. Conf. (Opt. Soc. Amer., 2016)*, Mar. 2016, Paper Tu3G. 5.

[14] S. Oda *et al.*, "In-band OSNR monitor using an optical bandpass filter and optical power measurements for superchannel signals," in *Proc. Eur. Conf. Exhib. Opt. Commun.*, Sep. 2013, pp. 1–3.

[15] Z. Dong *et al.*, "Modulation-format-independent OSNR monitoring insensitive to cascaded filtering effects by low-cost coherent receptions and RF power measurements," *Opt. Exp.*, vol. 23, no. 12, pp. 15971–15982, Jun. 2015.

[16] Z. Huang *et al.*, "A novel in-band OSNR measurement method based on normalized autocorrelation function," *IEEE Photon. J.*, vol. 10, no. 2, Apr. 2018, Art. no. 7903208.

[17] H. Lu, S. Cui, C. Ke, and D. Liu, "Automatic reference optical spectrum retrieval method for ultra-high resolution optical spectrum distortion analysis utilizing integrated machine learning techniques," *Opt. Exp.*, vol. 25, no. 26, pp. 32491–32503, Dec. 2017.